High-Resolution Structural Insights into the Heliorhodopsin Family

K. Kovalev[1,2,3,4,5†], D. Volkov[2,3†], R. Astashkin[1,4†], A. Alekseev[2,3,4,5†], I. Gushchin[4], J. M. Haro-Moreno[10], I. Chizhov[11], S. Siletsky[12], M. Mamedov[12], A. Rogachev[4,8], T. Balandin[2,3], V. Borshchevskiy[4], A. Popov[7], G. Bourenkov[9], E. Bamberg[4,6], F. Rodriguez-Valera[10], G. Büldt[4] and V. Gordeliy[1,2,3,4*]

[1]Institut de Biologie Structurale J.-P.Ebel, Université Grenoble Alpes-CEA-CNRS, Grenoble, France

[2]Institute of Biological Information Processing (IBI-7: Structural Biochemistry), Forschungszentrum Jülich, Jülich, Germany

[3]JuStruct: Jülich Center for Structural Biology, Forschungszentrum Jülich, Jülich, Germany.

[4]Reseach Center for Mechanisms of Aging and Age Related Diseases, Moscow Institute of Physics and Technology (National Research University), Dolgoprudny, Russia

[5]Institute of Crystallography, University of Aachen (RWTH), Aachen, Germany

[6]Max Planck Institute of Biophysics, Frankfurt am Main, Germany

[7]European Synchrotron Radiation Facility Grenoble, France

[8]Joint Institute for Nuclear Research, Dubna, Russia

[9]European Molecular Biology Laboratory, Hamburg unit c/o DESY, Hamburg, Germany

[10]Evolutionary Genomics Group, Departamento de Producción Vegetal y Microbiología, Universidad Miguel Hernández, San Juan de Alicante, Spain

[11]Institute for Biophysical Chemistry, Hannover Medical School, Hannover, Germany

[12]Belozersky Institute of Physical-Chemical Biology, Lomonosov Moscow State University, Moscow, Russia

†These authors contributed equally to the work

*Correspondence to: valentin.gordeliy@ibs.fr (V.G.)

Abstract

Rhodopsins are the most abundant light-harvesting proteins. A new family of rhodopsins, heliorhodopsins (HeRs), has recently been discovered. Unlike in the known rhodopsins, in HeRs the N-termini face the cytoplasm. The function of HeRs remains unknown. We present the structures of the bacterial heliorhodopsin 48C12 in two states at the resolution of 1.5 Å, whichhighlight its remarkable difference from all known rhodopsins. The interior of HeR'sextracellular part is completely hydrophobic, while the cytoplasmic part comprises a cavity (Schiff base cavity, SBC), surrounded by charged amino acids and containing a cluster of water molecules, presumably being a primary proton acceptor from the Schiff base. At acidic pH, a planar triangular molecule (acetate) is present in the SBC. Structure-based bioinformatic analysis identified 10 subfamilies of HeRs, suggesting their diverse biological functions. The structures and available data suggest an enzymatic activity of HeR-48C12 subfamily and their possible involvement into fundamental redox biological processes.

Significance Statement

We present high-resolution crystal structures of the bacterial heliorhodopsin 48C12, a representative of the recently discovered family of microbial rhodopsins. In opposite to all other rhodopsins, heliorhodopsins face the cytoplasm of the cells with their N-termini. The structures of two different states of 48C12 reveal specific features of heliorhodopsins, such as existence of a water-filled cavity in the cytoplasmic side near the retinal Schiff base, able to accommodateanions of triangular geometry, such as nitrate, carbonate or acetate, and completely hydrophobic organization of the inner extracellular part of the protein. Hence, the structure gives important insights into possible functions of 48C12.

Introduction

Microbial and animal visual rhodopsins (classified into type 1 and 2 rhodopsins correspondingly) comprise an abundant family of seven-helical transmembrane proteins that contain a covalently attached retinal cofactor[1–3]. Upon absorption of a photon, the retinal isomerizes, triggering a series of conformational transformations correlating with functional and spectral states known as the photocycle[4,5,6]. Microbial rhodopsins are currently considered to be universal and the most abundant on the Earth light harvesting proteins. Before 1999, only rhodopsins from halophilic archaea had been known. About 30 years after the discovery of the first rhodopsin (bacteriorhodopsin, bR)[2],the first non-haloarchaeal rhodopsin was reported (Neurospora rhodopsin, NR)[7]. Soon after that, metagenomics studies by Beja *et al.* led to the discovery in 2000 of a rhodopsin gene in marine Proteobacteria that was named accordingly proteorhodopsin (pR)[8]. Since then, seven thousand microbial rhodopsins were identified. They are present in all the three domains of life (bacteria, archaea and eukaryotes) as well as in giant viruses[4]. The discovery of channelrhodopsins[9] led to development of optogenetics, the revolutionary method for controlling cell behavior *in vivo*, in which microbial rhodopsins play the key role[10–13].

Several rhodopsins with new functions have recently been discovered and characterized. Among the members of the rhodopsin family are light-driven proton, anion and cation pumps, light-gated anion and cation channels, and photoreceptors[3,14–16]. Genomic and metagenomic studies dramatically expanded the world of rhodopsin sequences, some of which were found in unexpected organisms and habitats, for example, sodium-pumping rhodopsins (NaRs) in Flavobacteria[17,18] and the rhodopsins from giant viruses[19–21]. The widely spread presence and importance of pR-based phototrophy in the marine environment[22] was identified.Recently, rhodopsins that function as inward proton pumps were discovered[23,24].

Despite diversity of their functions and differences in the structures, all these rhodopsins are oriented in the membranes in the same way. Their N-termini always face the outside of the cells. In 2018,Pushkarev*et al*. discovered a new large family of rhodopsins, named heliorhodopsins (HeRs), facing the cytoplasmic space of the cell with their N termini[25]. It was found that they are present in Archaea, Bacteria, Eukarya and viruses.

The function of HeRsis not yet known[26,27]. Moreover, the structural data on HeRs is limited to the very recently reported model of archaeal heliorhodopsin (*Ta*HeR)[28]. Here we present two crystallographic structures of the heliorhodopsin 48C12, discovered in an actinobacterialfosmid from freshwater lake Kinneret[25], corresponding to two states of the

protein, both solved at 1.5 Å resolution. The structures show an astonishingly large difference between the organization of HeRs and other type I rhodopsins. For instance, the protein has a big cavity in the cytoplasmic part, containing the cluster of water molecules, which is likely to serve as proton acceptor from the retinal Schiff base (RSB). Ten of 48C12 amino acids are highly conserved within all heliorhodopsins, and we believe that its structure and the discussed mechanisms will be a basis for understanding this new abundant family, and also the evolution of rhodopsins in general.

Results

Structure of the heliorhodopsin 48C12 at neutral pH

48C12 was crystallized using the *in meso* approach similarly to our previous works[29]. Rhombic crystals appeared in two weeks and reached 150 μm in length and width with the maximum thickness of 20 μm. We have solved the crystal structure of 48C12 at pH 8.8 at 1.5 Å. The crystals of $P2_1$ symmetry contained two protomers organized in a dimer in the asymmetric unit (See SI Appendix, fig. S1, S2). The high-resolution structure reveals 233 water molecules and 31 lipid fragments.

Similarly to other type I rhodopsins, each 48C12 protomer has seven transmembrane α-helices, connected by three extracellular and three intracellular loops. However, some of the loops are relatively large and have certain secondary structure (Fig. 1). The extracellular AB-loop of 48C12 (residues 34-64) is ~40 Å long and forms a β-sheet with the length of ~17 Å (Fig. 1B). It extends in the direction of the second protomer of the dimer while remaining parallel to the membrane surface, and thus covers the extracellular surface of the nearby molecule (Fig. 1, See SI Appendix, fig. S1). The intracellular BC-loop comprises 14 residues (86-98) and forms an α-helix with the length of ~18 Å (Fig. 1C). Other loops and N- and C-termini, although not forming regular secondary structures, are well-ordered and therefore are completely resolved. The relative location of the α-helices is also altered in comparison with other microbial rhodopsins with known structure (See SI Appendix, fig. S3, S4). Particularly, the most notable differences occur in the helices A, D and E (See SI Appendix, fig. S4).

Dimerization interface of 48C12

48C12 protomers interact in the dimer via helices D and E (Fig. 1B, C; See SI Appendix, fig. S5), with a broad hydrophobic interface in the middle part (inside the membrane) and interactions between polar residues, specifically Asp127 and Tyr179’ at the extracellular and Tyr151 and Asp158’ at the cytoplasmic sides of the membrane. Tyr179’ side chain is

additionally connected through a hydrogen bond to the main chain of the AB-loop of the neighboring protomer (nitrogen of Thr44). The AB-loop itself almost does not interact directly with the neighbor protomer, although it is stabilized by several hydrogen bonds mediated by numerous water molecules located on the extracellular surface of the dimer.

Several well-ordered lipid molecules are present in the structure, surrounding the protein dimer (See SI Appendix, fig. S6). Two of them permeate the heliorhodopsin between helices E and F near the β-ionone-ring of the retinal cofactor with the hydrocarbon tails. Surprisingly, the pocket of the hydrocarbon chain comprises polar amino acids Asn207, Asn138 and one water molecule. Asn207 is also exposed to the surface of the extracellular part of the 48C12 protomer in the middle of the membrane and is highly conserved within HeRs.

The structures of the protomers within the 48C12 dimer are similar (RMSD between protomers 0.144 Å), however there are differences in the EF-loop organization, α-helical BC-loop location, and 3 Å displacement of the cytoplasmic end of helix A is observed (See SI Appendix, fig. S7). Consequently, positions of several residues inside the protomers are slightly varied. Since general features of the heliorhodopsin structure are the same in both molecules, we will describe mostly the protomer A. Nevertheless, we will also describe the differences between the protomers where appropriate.

Mechanism of topological inversion of heliorhodopsins

It is known that insertion and folding of membrane proteins is guided by the "positive-inside rule"[30]. Using the structure of 48C12, we analyzed the location of positively and negatively charged residues in the cytoplasmic and extracellular domains of the protein and compared it to bacteriorhodopsin (bR) (Fig. 2). Notably, in 48C12, all the positively charged residues are located exclusively at the cytoplasmic side of the protein, which is consistent with the "positive-inside rule"[30]. Importantly, some of these residues, such as Arg91, Lys218, Lys222, and Arg231, are highly conserved in the subfamily of 48C12 (See SI Appendix, fig. S8). In addition, unlike bR, HeR contains only negative amino acids in the extracellular polar part of the proteins, which is characteristic for this subfamily.Thus, we suggest that HeRs follow the "positive-inside and negative-outside rule" rather than just the "positive-inside rule".

Structure of the extracellular region

As heliorhodopsins are topologically inverted in the membrane relative to other type I rhodopsins, the extracellular part of 48C12 corresponds to the cytoplasmic part of classical

microbial rhodopsins, such as bR. However, in 48C12 the internal region, embedded in the extracellular leaflet of the lipid bilayer, is completely hydrophobic and does not comprise any charged or polar amino acids and solvent-accessible cavities (Fig. 3C, Fig. 4). Hereafter, we denote this part as the hydrophobic extracellular region. Nevertheless, several clusters of polar amino acids are located at the extracellular half of the protein inside the membrane, but on the outer surface of the protein. Helices A and G interact by hydrogen bonding of Gln26 with Ser242 and Trp246, while helices F and G are also connected by a hydrogen bond between Gln247 and Ser201. We suggest that these interactions support the internal hydrophobic configuration at the extracellular side. The absence of any charged or/and polar amino acids inside the region may explain the absence of any proton/ion pumping by 48C12[25].

Retinal binding pocket and cavity in the retinal Schiff base region

The retinal binding pocket of 48C12 (Fig. 1 and 2) is also different from that of microbial rhodopsins with known structures. Near the retinal molecule, helices C and D are connected by hydrogen bonding of Asn138 (analog of Asp115 in bR and Asp156 in ChR2) with Ser112 (analog of Thr90 in BR and Thr128 in ChR2) and Ser113. The Asn138 side chain is also stabilized by hydrogen bonding with Trp173 through a well-ordered water molecule (Fig. 3C). In the region of the β-ionone-ring of the retinal molecule, only two residues (Met141 and Ile142) are similar to those in bR (See SI Appendix, fig. S9). Although many of the residues of the pocket walls remain aromatic in 48C12, there are notable alterations such as for example Phe206 in the position of Trp182 in bR, Trp105 instead of Tyr83 and Tyr108 in the place of Trp86. All these residues are highly conserved in heliorhodopsins. Interestingly, polar Gln213 (in the position of Trp189 in bR) is located close to the β-ionone-ring.

The Schiff base is surrounded by an unusual, for the rhodopsins of type I, set of residues: for example, Ser237 replaces Asp212 (extremely conserved aspartate in type I rhodopsins), Glu107 replaces Asp85, His23 replaces Met20, the bulky Phe72 replaces Val49, Met115 replaces Leu93, Ser76 replaces Ala53. In this configuration, RSB is hydrogen-bonded directly to Glu107 (RSB counter ion) and Ser237. The Glu107 sidechain is stabilized by two serine residues (Ser76 and Ser111).

The distinctive feature of 48C12 heliorhodopsin is the presence of a large hydrophilic cavity in the vicinity of the Schiff base (Schiff base cavity, SBC) between residues Glu107 and Arg104 (analog of Arg82 in bR). The SBC is separated from the cytoplasmic bulk volume with the only side chain of Asn101 (Fig. 3) and is surrounded by polar residues Glu107,

His23, His80, Ser237, Glu230, Tyr92, Asn16, Asn101, Tyr108 and filled with 6 water molecules (Fig. 3B). The listed amino acids, together with the water molecules, create a dense hydrogen bonding network, which protrudes from the RSB to Arg104. The Arg104 side chain is pointed towards the cytoplasm and is stabilized by Glu230, Glu149 and also Tyr226. It should be noted that in protomer B there is an alternative conformation of Arg104, Glu230 and Tyr226, which, however, does not affect the shape of the cavity. The Glu149 side chain is additionally stabilized by Trp105 and by a water-mediated hydrogen bond to Gln216 and Gln213. The calculation of the hydrophilic/hydrophobic membrane boundaries shows that Glu149 is located out of the hydrophobic part of the membrane (Fig. 3A) and can be accessed from the cytoplasmic bulk, which is also proved by the cavities calculations using HOLLOW[31]. In protomer B, the accessibility of Glu149 from the bulk is lower, mostly because of slight alterations of the helices positions. Importantly, all the residues mentioned in this paragraph are highly conserved within all the known heliorhodopsins (See SI Appendix, fig. S8, S10). This fact together with their structural roles points towards their functional importance.

Role of the Schiff base cavity

As it was shown in previous studies, His23, His80 and Glu107 do not act as a proton acceptor group from the RSB, however His23 and His80 are important for proton transfer [25,26]. Our structure shows that the rechargeable amino acids E149 and E230 are connected to the RSB via a continuous network of hydrogen bonds, but have not yet been studied. To understand better their roles for the heliorhodopsin functioning, we produced E149Q and E230Q mutants and studied the properties of their photocycles. First of all, we should stress that these mutants were not stable during purification. Moreover, E230Q degrades quickly upon illumination even while remaining in the lipid membranes. It indicates that both amino acids are important for the protein stabilization. We measured the transient absorption of the mutants with the solubilized (not purified) protein (Fig. 3D). Formation of the K□M photocycle intermediate was observed for both mutants, therefore neither Glu149 nor Glu230 is the proton acceptor. However, the O_2-state decay in mutants is more than two times longer than that of the wild type protein (Fig. 3D), which indicates the involvement of Glu149 and Glu230 in the protein function. Thus, none of charged amino acids, surrounding the SBC, is a proton acceptor. Taking into account all facts (also the absence of charged amino acids in the hydrophobic extracellular internal part of the protein and that the proton is not transiently released to the aqueous phase[25]), we conclude that the only candidate for the proton acceptor is the water

cluster in the cavity. Indeed, water molecules were shown to play key role in functioning of microbial rhodopsins[32]. Thus, we suggest that proton is stored in the aqueous phase of the cavity after its release from the RSB and is returned to the RSB in the end of 48C12 photocycle.

To learn more about the movement of the charges inside the protein we performed time-resolved studies of electrogenic behavior of the protein. Upon the laser flash illumination (532 nm, 10 ns) of proteoliposomes containing 48C12 a generation of transmembrane electric potential was observed (See SI Appendix, fig. S11).The rise of the membrane potential corresponds to the outward transfer of the positive charge.We observed the major (~9 μs, ~70%) and the minor (~30 μs, ~30%) parts of the potential increase (See SI Appendix, fig. S11). The characteristic time of the first component coincides with the generation of the M-state and corresponds to deprotonation of the RSB in accordance with the photocycle (See SI Appendix, fig. S12, S13). The minor part may relate to spectroscopically silent conformational relaxation of the proton and charged residues upon the M-state formation triggered by deprotonation of the RSB. After that, a drop of membrane potential is observed. The first component of the drop (~0.5ms, ~10-20% of the maximum of the potential) coincides with the decay of the M- to the O_1-states, which corresponds to reprotonation of the RSB in accordance with the photocycle (See SI Appendix, fig. S12) and means the movement of the proton in the opposite direction. The next component of a complete decay of the electric potential (~500 ms) to zero correlates with the spectroscopic transitions from the O_1-to the precursor of the ground state (GS) (See SI Appendix, fig. S12, S13). It is accompanied by the movement of the charged residues to the ground state positions/states. Remarkably, the movement of the proton in 48C12 is very different from that in all the known proton pumps. Indeed, in the case of bR[33,34] and pR[35] similar experiments showed that upon proton translocation it always moves in one certain direction (inside proteoliposomes in case of bR) during the entire photocycle. In case of 48C12 the direction of the proton movement is reversed upon reprotonation of the RSB. The results of this time-resolved study are in favor of our hypothesis that the SCB plays the role of a collective primary proton acceptor.

Structure of 48C12 at acidic pH

While the biological function of HeRs remains unknown, thorough study of different 48C12 states is of great potential benefit for elucidating it. To investigate the conformational rearrangements in the heliorhodopsin associated with pH decrease, we also solved the crystal structure of 48C12 at 1.5 Å using the crystals grown at pH 4.3. Indeed, pH of the surrounding

solution affects the functionality and the structure of microbial rhodopsins due to protonation or deprotonation of the key residues [36–38]. Moreover, it was shown for bR that the structure of the protein at acidic pH is similar to that of its M-state [39]. Thus, analysis of heliorhodopsin structure at low pH may be of high importance for understanding of its biological function and possible rearrangements in protein structure during photocycle. While the crystal packing is the same as in the crystals grown at neutral pH, with one 48C12 dimer in the asymmetric unit, the crystals were colored blue (maximum absorption wavelength of 568 nm) at acidic pH, while at neutral pH they were violet (maximum absorption wavelength of 552 nm), which corresponds to the color of the wild-type protein in solution under the same conditions[26] (See SI Appendix, fig. S1). We designate these two 48C12 forms as blue and violet, respectively. The color shift is presumably caused by the protonation of the Glu107 residue[25]. Key differences between the two structures are shown in Fig. 5. In general, the backbone organization is the same at both acidic and neutral pH values (RMSD between models 0.158 Å), however the cytoplasmic parts of helices A and B are displaced for 1 to 2 Å, respectively, in the blue form (See SI Appendix, fig. S7).

At the cytoplasmic side, the main difference is observed in the organization of the water molecules inside the SBC (Fig. 5C). The hydrogen bonds network propagating from the RSB to Arg104 and Glu230 is present in both models. Interestingly, the difference F_o-F_c electron densities at 1.5 Å resolution indicate the presence of a triangular molecule in the SBC (See SI Appendix, fig. S14F). As the crystallization buffer contained only one molecule of triangular geometry, the acetate anion, the densities were fitted with an acetate (CH_3COO^-) molecule (Fig. 5, See SI Appendix, fig. S14E). It fits the density well; however, the acetate can mediate only two hydrogen bonds instead of three bonds necessary to fit the environment of two water molecules 3 and 5 and Glu107 (Fig. 5C, See SI Appendix, fig. S14C, D). Other molecules that could fit the triangular density and create three hydrogen bonds with water molecule 3 and 5 and Glu107 could be nitric acid (NO_3^-) or bicarbonate (HCO_3^-)(See SI Appendix, fig. S14C, D). This is in line with the very recent publication, where anion binding was shown in the 48C12 mutated at the Glu107 position[40]. Particularly, NO_3^-binding was demonstrated spectroscopically in the E107A and E107Q mutants, which imitate the wild type protein with the protonated (neutralized) Glu107.

Transient absorption spectroscopy of the 48C12 in the presence of acetate indicated that at neutral pH the anion does not affect the kinetics of the protein (See SI Appendix, fig. S12, S13). On the contrary, at pH 5.0 we observed ~1.5 times slowdown of the K□M-state decay

and ~2 times acceleration of the O_2-state formation (See SI Appendix, fig. S12, S13). We also observed a slight (1.5 nm) shift of the maximum absorption wavelength of the 48C12 in the presence of acetate at acidic, but not at neutral pH (See SI Appendix, fig. S12).The results of the spectroscopy experiments correlate nicely with the obtained model of the 48C12 at acidic pH. Indeed, the anion does not interact directly with the RSB, which may explain only the small shifts of the maximum absorption wavelength upon anion binding. At the same time, acetate is hydrogen-bonded to the neutralized Glu107 side chain, which is possible exclusively at low pH values.This explains the absence of any effects of the acetate on the spectra and kinetics of the 48C12 at neutral pH. Therefore, the structure of 48C12 at acidic pH reveals the structural basis of anion binding in the core of the protein and show the ability of the heliorhodopsin to bind the molecules of triangular geometry in the SBC.

While at neutral pH RSB is stabilized through hydrogen bonding to Ser237 and Glu107, at acidic pH it is still bound to Glu107, however is slightly shifted towards Ser111, thus weakening the connection to Ser237 (Fig. 5D). Ser76 is in a single conformation at acidic pH, and does not stabilize Glu107 anymore. Ser237 flips from the RSB towards the cavity at the cytoplasmic part of the protein (Fig. 5D). At the same time, His23 is reoriented compared to the structure at neutral pH, and forms a hydrogen bond with Ser76 in the blue form. The reorientation of His23 may be caused either by protonation of Glu107[25] or by protonation of His23 itself, or the combination of these events. Nevertheless, the reorientation of His23 towards the extracellular side in the blue form of HeRs results in loss of the water molecule, which is coordinated by Gln26 in the purple form (Fig. 2C). The organization of the Ser242-Gln26-Trp246 cluster, located at the extracellular half of the protein surface inside the hydrophobic membrane, is also disturbed (Fig. 5B). Prominently, Trp246, conserved in most HeRs (See SI Appendix, fig. S8, S10) and exposed to the surrounding lipid bilayer, loses the hydrogen bond to Gln26 and reorients in the blue form of 48C12. Such reorientation might trigger a signal transduction cascade, if heliorhodopsins are light sensors[25], similarly to sensory rhodopsins II, where there is also an aromatic amino acid in the helix G, Tyr199, which controls the signal transducer protein[41]. Alternatively, a latch-like motion of Trp246 might create a defect in the surrounding lipid membrane and open a pathway towards Gln26, His23 and the retinal.

Comparison of the structures of the archaeal and bacterial heliorhodopsins

Very recently, the structure of the archaeal heliorhodopsin *Ta*HeR at 2.4 Å resolution was reported by Shihoya *et al*[28].Thisallowed us to compare HeRs from different origin.

In general, structures of 48C12 and *Ta*HeR are similar, with the RMSD between models of 0.66 Å (See SI Appendix, fig. S15A,B). Both proteins form dimers in the lipid bilayer. The most notable differences occur in the AB-loop localization, whose β-turn in case of 48C12 is moved closer to the nearby protomer (See SI Appendix, fig. S15C).The DE-loop is slightly longer in 48C12 and is displaced by around 9 Å in comparison to *Ta*HeR (See SI Appendix, fig. S15C).

The organization of the inner parts of both proteins is also similar (See SI Appendix, fig. S15F). Side chains of Arg104 (Arg105 in *Ta*HeR), Glu107 (Glu108 in *Ta*HeR), Glu230 (Glu227 in *Ta*HeR), Glu149 (Glu150 in *Ta*HeR), Tyr217 (Tyr214 in *Ta*HeR) are slightly different in the models, however, the overall configuration is similar (See SI Appendix, fig. S15F). The polar cavity,similar to the SBC of the 48C12, is found in *Ta*HeR near the RSB and filled with water molecules. It should be noted that the number of waters inside the proteins (and particularly in the cavity) and also those bound at the protein surface is much higher in the model of 48C12, most probably due to higher resolution of the model.

Surprisingly, the structure of 48C12 revealed similar fenestration on the surface of the protein, as that found in *Ta*HeR (See SI Appendix, fig. S6, S15D,E). As described in more details in [28] and in the section "*Dimerization interface of 48C12"* of the present manuscript, the fenestration is occluded by the hydrocarbon chain in both proteins. However, in case of the archaeal protein, lipid molecule goes through the fenestration, while in 48C12 the end of the hydrocarbon chain is well-ordered in the concavity (See SI Appendix, fig. S6). Thus, the fenestration is tighter in case of 48C12, presumably due to the presence of two bulky hydrophobic residues, Ile170 and Phe203, and the positions of Phe172 and Ala200 of the *Ta*HeR (See SI Appendix, fig. S15D, E).

Structure-based bioinformatic analysis of heliorhodopsins

The structures of 48C12 allowed us to identify amino acid residues, comprising the key regions of the heliorhodopsin (Fig. 6). Based on the comparison of these amino acids in different HeRs, we classified heliorhodopsins in ten subfamilies with potentially different properties. The subfamilies are presented in a phylogenetic tree (See SI Appendix, fig. S16). The groups that contain less than 10 members were merged into "Unsorted proteins".

The group of 48C12 (subfamily 1) is the largest and comprises 195 proteins out of the 479 unique sequences of HeRs currently available[25,42]. The majority of HeRs of subfamily 1 have bacterial origin, with most of them from *Actinobacteria*. However, representatives of the

subfamily are also found in *Chloroflexi* and *Firmicutes* of the *Terrabacteria* group, and also in *Proteobacteria* and the PVC group. The host of the unique protein A0A0L0D8K8 is a eukaryote *Thecamonastrahens*. Importantly, the sequences belong to both gram-positive and gram-negative bacteria, which is inconsistent with thepreviously made conclusion[27].

Those residues that are conservative in the most of the proteins were identified (See SI Appendix, fig. S10). The alignment of 10 most distinct heliorhodopsins of subfamily 1 is shown in SI Appendix, fig. S17. Using the structure of 48C12 as a reference, we identified the following regions of protein comprised of conserved residues as potentially important for the function of 48C12 and correspondingly for the whole 48C12 subfamily and in some cases for all HeRs (Fig. 6).

Namely, heliorhodopsins have a conservative pattern of the residues that stabilize the RSB (Ser237, Glu107, Ser111 and Ser76) (See SI Appendix, fig. S17, S18). The SBC and surrounding it charged and polar residues (His23, His80, Asn101, Tyr108, Asn16, Glu230, Arg104, Tyr92), together with residues Leu12, Leu96, and Leu227, forming a hydrophobic barrier between the cavity and the cytoplasm, are almost completely conserved in subfamily 1 (See SI Appendix, fig. S17, S18). The polar region near Glu149 and Arg104 is also conserved (Glu149, Gln216, Tyr226, Trp105, Gln213) (See SI Appendix, fig. S17, S18). We found that the common feature of heliorhodopsins is the hydrophobic organization of the extracellular internal part (Fig. 3, See SI Appendix, fig. S17, S18). Indeed, only a few heliorhodopsin subfamilies have members with charged or polar residues in this region. This fact is very interesting from the functional point of view and will be discussed in the following paragraphs. As it was already mentioned, 48C12 has three clusters comprised of polar residues (Gln26/Ser242/Trp246, Gln247/Ser201 and Ser112/Ser113/Asn138/Trp173), which are structurally important presumably for the interactions between the helices and for stabilization of the protein. Importantly, many residues of the characteristic for 48C12 long AB-loop and dimerization interface are conserved within subfamily 1. To determine whether the same regions and residues are conserved within other HeR subfamilies, we performed additional bioinformatic analysis of the whole family.

Comparison of heliorhodopsins subfamilies

The most conservative residues in HeR family are similar to those of subfamily 1 with some variations. The filling of the cytoplasmic part, particularly the RSB region, the SBC, the hydrophobic barrier separating the cavity from the cytoplasm, the region near Glu149, as well

as the hydrophobic extracellular configuration are highly conserved within all HeRs (See SI Appendix, fig. S8, S10). These regions include such polar and charged residues as Ser237, Glu107, Ser111, Ser76, His23, His80, Asn101, Tyr108, Asn16, Glu230, Arg104, Tyr92, Glu149, Gln216, Tyr226, Trp105 and Gln213, which were shown to be structurally important in 48C12 (See SI Appendix, fig. S8, S10). Indeed, only a few heliorhodopsin subfamilies have variations in the listed parts (See SI Appendix, fig. S19). It should be noted, that although Gln213 is almost completely conserved among heliorhodopsins of subfamily 1, methionine is an often variant for this position in heliorhodopsins. In addition, the analogues of the residues, comprising the clusters at the surface of 48C12 (Gln26/Ser242/Trp246 and Gln247/Ser201) are present in most of the HeRs.

The differences between heliorhodopsin subfamilies were identified by a comparison of the residues, comprising structurally important regions in 48C12. In general, amino acids responsible for dimerization are not conserved in all HeRs. However, in most cases analogues of Tyr179 and Asp127 are present (except subfamily 2), but hydrophobic residues of the dimerization interface are different in almost all the groups. The AB-loop is conserved only within some subfamilies, but varies notably from group to group in size and amino acid composition. Despite this, residue Pro40 is highly conserved among all HeRs and is part of a β-sheet of the AB-loop of 48C12.

Subfamily 2comprises 19 members and mostly consists of viral proteins, but there are two representatives of *Euryarchaeota*; the bacterial *PVC* group and eukaryota are also presented with 1 protein. We found that this group is the most distinct from all others especially in the organization of the extracellular part and the retinal binding pocket. Interestingly, one of the members of this group has two Asn residues near the cytoplasmic inner cavity in the positions of His23 and His80 of 48C12. A lot of its members have glutamate in helix F in the position of Leu202 in 48C12, which belongs to its hydrophobic extracellular part. There are no analogues in microbial rhodopsins for Glu202, which thus may be a key determinant of the subfamily 2 protein function. A highly conserved Pro172, which makes a π-bulge in helix E of 48C12, also characteristic only for HeRs, is absent in group 2, however, proline is present in position 168 (helix E) of 48C12 in almost all its members. This alteration may change the shape of helix E and affect the folding of the protein. The retinal binding pocket in HeRs of group 2 is extremely different from that of other subfamilies, especially due to the presence of positively charged His residues in positions 162 and 166 of the reference protein 48C12. Analogues of Asn138 are also absent in group 2.

Subfamilies 3, 4, 5,have variations from 48C12 in the retinal binding pocket. Particularly, methionine and asparagine in subfamily 3 are placed in the positions of Gln213 and Ile142 of 48C12, respectively. The same asparagine is present in groups 4 and 5, however, it alternates with asparagine in the position of Asn138, thus only the Asn residue is present near the β-ionone ring of the retinal.

Subfamilies 7, 8 and 9 have a very interesting feature of conservative Tyr in position 202 of 48C12. Asn is present in the position of Ile142 of 48C12 in all members of groups 8 and 9 and in some representatives of subfamily 7. Group 9 also has no analogues of Asn138 of 48C12.

"Unsorted proteins" group includes the most different heliorhodopsins (See SI Appendix, fig. S20). These proteins presumably maintain the polar cavity in the cytoplasmic part, however, its surroundings are varied. Most interesting, in subgroup U1, histidine is present in the position of Asn16 in addition to two histidines in the positions of His23 and His80 of 48C12. Moreover, at the extracellular side two glutamates are present in all members of subfamily U1 in the positions of Leu73 and Ile116 of 48C12. Glutamate is also found in the positions of Pro172 (subfamily U2), Val69 and Leu202 (subfamily U8) of 48C12. Positively charged residues also appear in the extracellular side of the members of subfamilies U1, U6, U7, and U11, such as His residues in the position of Leu73 and Arg and Lys residues in the position of Leu253 of 48C12. The positions of 48C12, whose analogues in other HeRs are occupied by unusual charged or polar residues and possible variants of those residues are shown in Fig. 6. These charged amino acids, especially located in the extracellular part of the proteins, may be crucial for the functions of those HeRs.

Subfamilies 3, 5, 6, 8, U1, U2, U3, U4, U5, U6 and U12 consistexclusively of bacterialproteins. Subfamilies 4, 7, 9, and U13 represent archaeal HeRs (except one bacterial protein from subfamily 4 and one from subgroup U13), mostly *Euryarchaeota*, but subfamily 7 also has members of *Asgard* and *TACK* groups. Subfamilies U8, U9, U11 comprise proteins of eukaryotic origin.

Discussion

Molecular mechanisms and biological function(s) of HeRs.

The biggest surprise of the first studies of HeRs (the studies of 48C12) is that the attempts to identify amino acids playing the roles of primary proton acceptor and proton donor to the RSB failed[25,26]. Such amino acids are key functional determinants in all known rhodopsins.

Another important fact is that Pushkarev *et al*. did not observe any translocation of the proton (an ion) through the protein to its polar surfaces. High-resolution crystallographic structures of 48C12 HeR, which represents the most abundant subfamily of HeRs (195 out of 479 currently known unique sequences), were solved at 1.5 Å resolution with the crystals obtained at pH 8.8 and 4.3, respectively. The structures correspond to the two different forms of the protein. Both structures show remarkable difference between HeRs and all the known rhodopsins. The retinal binding pocket and the parts of the cytoplasmic and extracellular regions of the protein, which are determinants of the function of the known rhodopsin, are also different. There is no analogue to this protein amongother type 1 (microbial) and type 2 (visual) rhodopsins.

In the cytoplasmic part of the protein, at pH 8.8, a large cavity (SBC)is located close to the RSB and surrounded by highly conservative charged amino acids His23, His80, Arg104, Glu107, Glu230, the protonated RSB, by polar residues Asn16, Tyr92, Asn101, Tyr108, Ser237 and filled with 6 water molecules. The amino acids and the RSB are interconnected by an extensive hydrogen network mediated by the water molecules (Fig. 2). There are two pathways from the cavity to the bulk. From one of the sides the cavity is separated from the bulk by only the Asn101 residue, foundon the surface of the protein at the level of the hydrophobic/hydrophilic interface (Fig. 4, See SI Appendix, fig.S21). From the other side, the cavity is delineated by Arg104, found in almost all rhodopsins as a major gate between the RSB and the bulk.

The major difference between the two structures is that at lower pH the SBC comprises planar triangle-shaped molecule in the cavity. Remarkably, several residues mentioned above (namely His23, His80, Arg104, Glu107, Tyr108, Ser237) were subjected to alanine substitution[26] which in all cases led to the changes of absorption spectra. This result supports the presence of a strong interaction of the SBC with the RSB. In its turn, this means that isomerization of the retinal modifies the properties of the SBC since the base is directly connected to the cavity through Glu107 via a hydrogen bond (Fig. 3B, Fig. 5D).

The structure also suggests why the previous attempts to identify the proton acceptor and the proton donor have failed[25,26]. One of the reasons is that one of the possible amino acid candidate for these roles, for instance, Glu230, which is the key member of the active site, was overlooked in the previous studies because of poor prediction of the protein topology in the membrane (Fig. 1 in ref [26]). However, additional mutational analysis suggests that the cluster of water molecules in the SBC plays a role of a reservoir for the proton dissociated from the RSB. Importantly, the transfer of the RSB proton to the hydrophobic extracellular

part of the protein upon isomerization of the retinal seems to be problematic due to high free energy penalty. We suppose that the RSB proton dissociates upon isomerization of the retinal, but does not leave the SBC during the photocycle. We also suggest that the SBC may play the role of an 'active site' for substrate binding inside 48C12. In the latter case, theproton released from RSB during the photocycle might interact with the substrate in the reaction H^+ + substrate$^-$ → reduced substrate, like in carbon fixation, which is known as one of the most important biosynthetic processes in biology[43].

Since the extracellular part of the protein is highly hydrophobic the transfer of the RSB proton upon isomerization of the retinal to this part of the protein is energetically unfavorable. It means that, in opposite to bR, the RSB proton of 48C12 does not follow the RSB upon retinal isomerization, but dissociates from the base and remains in the cytoplasmic part of the protein and is temporarily accommodated in the cavity. Then the proton moves back upon reisomerization of the retinal and reprotonates the RSB.

Biological role of HeR Subfamily 1

At this point it is difficult to establish the primary role of HeR even of the best studied Subfamily 1. Pushkarev*et al.* suggested that HeRs may function as sensory proteins[25]. This conclusion was basedon two observations. First, the authors did not detect any ion translocation activity of the protein (under experimental conditions corresponding to pH 8.1). Second, the photocycle of the protein (measured at pH 8.5) was several seconds long, which is characteristic for sensory rhodopsins[3]. Along these lines, we noted above that heliorhodopsin possesses a hydrogen bond-forming aromatic amino acid Trp246 that faces the membrane and that might change its conformation under illumination, similarly to Tyr199 in *Np*SRII[41,44]. Usually, the genes of sensory rhodopsins have a gene coding for a signal transducer protein, located nearby and often co-transcribed[45,46]. At present, two distinct types of sensory rhodopsins are known: SRII-like photoreceptors utilize transmembrane chemoreceptor-like transducer proteins, whereas *Anabaena* sensory rhodopsin (ASR) utilizes a soluble transducer protein that dissociates from ASR upon illumination[3]. In case of subfamily 1, however, no conserved proteins, which could potentially be signal transducers, could be detected in the genomic neighborhood. On the other hand, in some microbes (aquatic actinobacteria such as the marine *Ca. Actinomarina*) that most often contain heliorhodopsins, their genes are surrounded by two large clusters of Nuo genes (See SI Appendix, fig. S22), the products of which are the key proteins in respiratory chains. At this point, it is unclear what this might mean. However, the ability of HeRs to bind the triangular anions like carbonate in the SBC suggests the possibility of its involvement in carbon fixation.

The analysis of the presence/absence of HeRs in monoderm and diderm representatives of the Tara Oceans and 25 freshwater lakes metagenomes led to the conclusion that heliorhodopsins were absent in diderms, confirming their absence in cultured *Proteobacteria*. Judging by a specific semipermeability of outer membranes of diderms, the authors proposed a role of HeRs in light-driven transport of amphiphilic molecules[27]. However, the structures of 48C12 do not support such function for HeRs. Moreover, according to the literature data, we conclude that, in fact, there is no clear evidence of the HeRs presence only in monoderms[47]. For example, some of the proteins of subfamily 1 are originating from *Bacteroidetes*, *Gemmatimonadetes* and from *Proteobacteria*, all of which are assumed to be diderms. Some HeRs from other subfamilies are found in the phyla *Thermotogae* and *Dictioglomy*, which also have diderm cells.

Although at this point we cannot provide a definitive role for HeR, we would like to advance a hypothesis. In many (if not most) cases,heliorhodopsins are found in pelagic microbes living in the photic zone of aquatic habitats (freshwater or marine). They appear in microbes that often contain also a classical rhodopsin, typically a proton pump, providing the cell with unlimited energy as long as there is light. The transfer of the proton from the retinal to the interior of the cell, likely reducing a molecule of carbonate or nitrate, might act like cyanobacterial (or plant) photosystem II, transforming light energy into reducing power to form precursors of cell biomass. This would transform the microbes containing the two kind of rhodopsins in primary producers like cyanobacteria, and would help explaining the extraordinary success of some of them, such as the actinobacteria that are the most abundant microbes in most photic freshwater habitats. Further structure-guided functional studies are necessary to clarify the biological role (roles) of this unusual family of rhodopsins.

Materials and Methods

Protein expression and purification

The gene of helirhodopsin 48C12 (UniProt ID A0A2R4S913; NIH Genbank AVZ43932.1) was synthesized *de novo* and optimized for expression in *E.coli* with Thermo Fisher Scientific GeneOptimizer service. The optimized gene was introduced into Staby™Codon T7 expression plasmid system (Delphi Genetics, Belgium) via NdeI and XhoI (Thermo Fisher Scientific) that led to the addition of 6×His tag to the C-terminus of the gene. The resulting plasmid DNA was sequenced (Eurofins Genomics, Germany) and used to transform *E.coli* C41 strain.

The protein expression procedure is adopted from ref [48] but slightly modified. The culture was cultivated at 37 °C in the auto induction media (1% w/v Trypton, 0.5% w/v Yeast extract, 0.5% w/v glycerol, 0.05% w/v glucose, 0.2% w/v lactose, 10 mM $(NH_4)_2SO_4$, 20 mM KH_2PO_4, 20 mM Na_2HPO_4, adjusted pH 7.8) containing 150 µg/ml of ampicillin antibiotic to OD_{600}=0.8. After, the cultivation temperature was decreased to 26 °C with subsequent addition of 150 µg/ml ampicillin, 20 µM all-trans Retinal (solubilized in Triton X-100 detergent) and 0.1mM IPTG and the culture was grown overnight. The concentration of antibiotic after induction was maintained with addition of extra 150 µg/ml each two hours.

The cells were then collected and disrupted at 20000psi with M-110P homogenizer (Microfluidics) in the buffer containing 30mM Tris-HCl pH 8.0, 0.3M NaCl, 0.04% Triton X-100, 50 mg/L DNase I (Sigma-Aldrich) and cOmplete® protease inhibitor cocktail (Roche). The total cells' lysate was ultracentrifugated at 120000 rcf. Then, membranes were isolated and dispensed in the same buffer without DNAse (whit addition of 1% w/w DDM detergent and 5mM all-trans retinal) and stirred overnight at 4 °C.

The non-soluble fraction was separated by ultracentrifugation at 120,000 rcf for 1 h at 4 °C. The resulting soluble protein mixture was loaded to Ni-NTA resin (Cube Biotech). The column with loaded resin was washed with 3 CV of washing buffer WB1 (30 mMTris-HCl pH 8.0, 0.3 M NaCl, 10 mM Imidazole, 0.05% Triton, 0.2% DDM) and washing buffer WB2 (30 mMTris-HCl pH 8.0, 0.3 M NaCl, 50 mM Imidazole, 0.05% Triton, 0.2% DDM). Then, heliorhodopsin was eluted with EB buffer (30 mMTris-HCl pH 7.8, 0.3 M NaCl, 250 mM L-Histidine (AppliChem), 0.05% Triton, 0.1% DDM). The eluted protein mixture was subjected to the size-exclusion chromatography column Superdex200 Increased 10/300 GL (GE Health Care Life Sciences) pre-equilibrated with SEC buffer (30 mMTris-HCl, 50 mMNaPi pH 7.8, 300 mMNaCl, 0.5 mM EDTA, 2 mM 6AHA (6-Aminohexanoic Acid), 0.075% DDM). The fractions were analyzed and those containing the 48C12 rhodopsin with peak ratio of ~1.25 and lower were collected and protein was concentrated to 20 mg/ml with 50 kDa concentration tubes at 5000 rcf and flash-cooled with liquid nitrogen.

Flash photolysis setup

The laser flash photolysis was similar to that described by Chizhov et al. [49–51] with minor differences. The excitation system consisted of Nd:YAG laser Q-smart 450mJ with OPO Rainbow 420-680nm range (Quantel, France). Samples were placed into 5x5mm quartz cuvette (Starna Scientific, China) and thermostabilized via sample holder qpod2e (Quantum Northwest, USA) and Huber Ministat 125 (Huber Kältemaschinenbau AG, Germany). The detection system beam emitted by 150W Xenon lamp (Hamamatsu, Japan) housed in LSH102 universal housing (LOT Quantum Design, Germany) passed through pair of Czerny–Turner monochromators MSH150 (LOT Quantum Design). The received monochromatic light was detected with PMT R12829 (Hamamatsu). The data recording subsystem represented by a pair of DSOX4022A oscilloscopes (Keysight, USA). The signal offset signal was measured by one of oscilloscopes and the PMT voltage adjusted by Agilent U2351A DAQ (Keysight). The absorption spectra of the samples were measured before and after each experiment on Avaspec ULS2048CL fiber spectrophotometer paired with AVALIGHT D(H)S Balanced light source (Avantes, Netherlands).

Preparation of samples for flash photolysis

The wild type protein sample (WT) for flash photolysis assay was purified in the same manner as for crystallization but with increased from 0.3 M to 0.6 M NaCl concentration on each purification step. The purified WT protein was 100x diluted in buffer containing 30 mM HEPES pH 7.0, 1 M NaCl, 2% DDM to concentration of ca. 0.5 mg/ml. The measurement was performed in the following way. The 350 ul sample was placed into the 5 mm light path cuvette and the temperature of the sample was set to 20^0C. After, the protein sample was exposed to 6 ns pulse of 3.5 mJ mean (standard deviation 6% on 1000 pulses) @545 nm. The transient absorption changes data was recorded (in 350-700nm light range; step 10nm) from 1mks up to 5 sec with two oscilloscopes with overlapping ranges (range ratio 1:1000) and averaged for 20 pulses for each wavelength. The data compression reduced the initial number of data points per trace to ca. 900 points. The samples of E230Q and E149Q mutant proteins were prepared without purification similar to [26] with modification. The E.coli C41 cells were disrupted at 20000psi with M-110P homogenizer in buffer containing 30mM Tris-HCl pH 8.0, 1 M NaCl and DNase I and non-soluble fraction was sedimented at 120000 rcf. The 5 g of the membranes were then washed and resuspended in 20ml of the buffer containing 30mM HEPES pH 7.0, 1M NaCl. After homogenization, the 2% DDM were added to 1.6ml of suspension and the sample was incubated for 30 min at 4 ^{0}C. Later, samples were applied to the centrifugation (for 10 min at 4^0C, 15000 rcf) and supernatant was collected for characterization. The flash photolysis measurement of E230Q/E149Q mutant-containing samples was performed at 400-610nm (step 70nm; each reading averaged for 20 pulses) at 20 ^{0}C using 6 ns excitation pulses of 3.5 mJ @545 nm.

Proteoliposomes preparation

Liposomes were produced from asolectin (20mg/ml Sigma, type IVS, 40% w/w phosphatidylcholine content) by sonication (at 22 kHz, 60 μA) for 2 min in 1 ml of 25 mM HEPES-NaOH buffer, pH 7.5. Reconstitution of the protein into liposomes was carried out by mixing the liposomes with protein in 1.5% (w/v) OG at the lipid/protein ratio of 100:1 (w/w) for 30 min in the dark. Removal of detergent was performed according to using Bio-Beads SM-2 absorbent (Bio-Rad). The detergent was removed by addition of a 20-fold excess of Bio-Beads (by weight) and stirring the suspension for 3 h at room temperature.

Electrometric time-resolved measurements of the membrane potential

Generation of the transmembrane electric potential difference ΔΨ was studied using a direct electrometric setup with time resolution of 100 ns as described in [33,34]. This technique includes fusion of the proteoliposomes with the surface of a collodion phospholipid-impregnated film (a membrane) separating two sections of the measuring cell filled with a buffer solution. The membrane should be thin enough and possess large electric capacitance (about 5 nF) for detecting fast charge translocation events. A pulsed Nd-YAG laser (YG-481, Quantel, λ = 532 nm, pulse half-width 12 ns, flash energy up to 40 mJ) was used as a source of flashes. In the process of the light-driven proton transfer, 48C12 creates ΔΨ across the vesicle membrane, which is proportionately divided with the measuring membrane and thus can be detected by Ag+/AgCl electrodes immersed in a solution at different sides of themembrane. Typically, themeasuringmembrane has high resistance of 2–3 GOhm, and the light-inducedΔΨdecays with a time constant of several seconds generation.

Crystallization

The crystals were grown with an *in meso* approach[44,52], similar to that used in our previous work[18,29]. The solubilized protein in the crystallization buffer was mixed with pre-melted at 42°C monoolein (Nu-Chek Prep) to form a lipidicmesophase. The 150 nl aliquots of a protein–mesophase mixture were spotted on a 96-well LCP glass sandwich plate (Marienfeld) and overlaid with 500 nL of precipitant solution by means of the NT8 crystallization robot (Formulatrix). The best crystals of the violet form were obtained with a protein concentration of 20 mg/ml and the precipitant solution of 2.0 M Ammonium Sulfate, 0.1 M Tris-HCl pH 8.8. For the blue form the best crystals were grown with the same protein concentration of 20 mg/ml and the precipitant solution of 2.0 M Ammonium Sulfate, 0.1 M Sodium acetate pH 4.3. The crystals were grown at 20°C to observable size in two weeks for the both types. The rhombic-shaped crystals reached 150 μm in length and width with maximum thickness of 20 μm. Crystals of the both forms were incubated for 5 min in cryoprotectant solution (2.0 M Ammonium Sulfate, 0.1 M Tris-HCl pH 8.8 for the violet form and 2.0 M Ammonium Sulfate, 0.1 M Sodium acetate pH 4.3 for the vlue form supplied with 20% (w/v) glycerol) before harvesting. All crystals were harvested using micromounts (MiTeGen), and were flash-cooled and stored in liquid nitrogen. Absorption spectra from the 48C12 crystals were measured at ID29s beamline of European Synchrotron Radiation Facility (ESRF), Grenoble, France at 300 K[53].

Collection and treatment of diffraction data

X-ray diffraction data were collected at Proxima-1 beamline of the SOLEIL, Saint-Aubin, France at 100 K, with an EIGER 16M detector and at P14 beamline of the PETRAIII, Hamburg, Germany France at 100 K, with an EIGER 16M detector. We processed diffraction images with XDS[54]and scaled the reflection intensities with AIMLESS from the CCP4 suite[55]. The crystallographic data statistics are presented in SI Appendix, Table S1. The molecular replacement search model was generated by RaptorX web server[56] based on the ESR structure (PDB ID 4HYJ[6]). Initial phases were successfully obtained in $P2_1$ space group by the molecular replacement using phenix.mr_rosetta[57] of the PHENIX[58] suite. The initial model was iteratively refined using REFMAC5[59], PHENIXand Coot[60]. The cavities were calculated using HOLLOW[31]. Hydrophobic-hydrophilic boundaries of the membrane were calculated using PPM server[61].

Bioinformatics analysis

Multiple amino acid alignment was performed using Clustal Omega algorithm[62]. Heliorhodopsins database was downloaded from InterPro[42] and merged with database provided in original article[25]. Phylogenetic tree was constructed and classes identified using iTOL server software version 4.3.2[63]. For removing those proteins above certain similarity threshold we used CD-HIT suite[64]. Cut-off similarity threshold is always specified. Calculations of conservative amino acids were performed using an in-house C# application written using Visual Studio Community 2017. Most conservative regions were identified and normalized results were visualized using in-house Wolfram Mathematica Notebooks.Genome sequence of the single-amplified genome AG-333-G23, belonging to the marine Ca. Actinomarinales group, was downloaded from the NCBI database (Biosample: SAMN08886063). Encoded genes were predicted using Prodigal v2.6[65]. tRNA and rRNA genes were predicted using tRNAscan-SE v1.4[66], ssu-align v0.1.1[67] and meta-rna[68]. Predicted protein sequences were compared against the NCBI nr database using DIAMOND[69], and against COG[70] and TIGFRAM[71] using HMMscan v3.1b2[72] for taxonomic and functional annotation. A custom database containing both type I and type III rhodopsins[25] was used to identify putative homologs. Resulted significative genes (HMMscan, E-value 1e-15) were then confirmed by determining the secondary structure and the presence of domains with InterPro[42].

References and Notes

1. Shalaeva, D. N., Galperin, M. Y. & Mulkidjanian, A. Y. Eukaryotic G protein-coupled receptors as descendants of prokaryotic sodium-translocating rhodopsins. *Biol. Direct* (2015). doi:10.1186/s13062-015-0091-4

2. Oesterhelt, D. & Stoeckenius, W. Rhodopsin-like protein from the purple membrane of Halobacterium halobium. *Nat. New Biol.***233**, 149–152 (1971).

3. Gushchin, I. & Gordeliy, V. Microbial Rhodopsins. in 19–56 (2018). doi:10.1007/978-981-10-7757-9_2

4. Beja, O. & Lanyi, J. K. Nature's toolkit for microbial rhodopsin ion pumps. *Proc. Natl. Acad. Sci.* (2014). doi:10.1073/pnas.1405093111

5. Ernst, O. P. *et al.* Microbial and animal rhodopsins: Structures, functions, and molecular mechanisms. *Chemical Reviews* (2014). doi:10.1021/cr4003769

6. Gushchin, I. *et al.* Structural insights into the proton pumping by unusual proteorhodopsin from nonmarine bacteria. *Proc. Natl. Acad. Sci.* (2013). doi:10.1073/pnas.1314549110

7. Bieszke, J. A., Spudich, E. N., Scott, K. L., Borkovich, K. A. & Spudich, J. L. A eukaryotic protein, NOP-1, binds retinal to form an archaeal rhodopsin-like photochemically reactive pigment. *Biochemistry* (1999). doi:10.1021/bi9916170

8. Beja, O. *et al.* Bacterial rhodopsin: Evidence for a new type of phototrophy in the sea. *Science (80-.).***289**, 1902–1906 (2000).

9. Nagel, G. *et al.* Channelrhodopsin-2, a directly light-gated cation-selective membrane channel. *Proc. Natl. Acad. Sci.* (2003). doi:10.1073/pnas.1936192100

10. Deisseroth, K. *et al.* Next-generation optical technologies for illuminating genetically targeted brain circuit. *J Neurosci.* (2010). doi:10.1523/JNEUROSCI.3863-06.2006.Next-Generation

11. Bamann, C., Nagel, G. & Bamberg, E. Microbial rhodopsins in the spotlight. *Current Opinion in Neurobiology* (2010). doi:10.1016/j.conb.2010.07.003

12. Nagel, G. *et al.* Light activation of Channelrhodopsin-2 in excitable cells of caenorhabditis elegans triggers rapid behavioral responses. *Curr. Biol.* (2005). doi:10.1016/j.cub.2005.11.032

13. Boyden, E. S., Zhang, F., Bamberg, E., Nagel, G. & Deisseroth, K. Millisecond-timescale, genetically targeted optical control of neural activity. *Nat. Neurosci.* (2005). doi:10.1038/nn1525

14. Govorunova, E. G., Sineshchekov, O. A., Li, H. & Spudich, J. L. Microbial Rhodopsins: Diversity, Mechanisms, and Optogenetic Applications. *Annu. Rev. Biochem.* (2017). doi:10.1146/annurev-biochem-101910-144233

15. Kandori, H. Ion-pumping microbial rhodopsins. *Frontiers in Molecular Biosciences* (2015). doi:10.3389/fmolb.2015.00052

16. Ernst, O. P. *et al.*Microbial and Animal Rhodopsins: Structures, Functions, and Molecular Mechanisms. *Chem. Rev.* (2014). doi:10.1021/cr4003769

17. Kwon, S. K. *et al.* Genomic makeup of the marine flavobacterium Nonlabens (Donghaeana) dokdonensis and identification of a novel class of rhodopsins. *Genome Biol. Evol.* (2013). doi:10.1093/gbe/evs134

18. Gushchin, I. *et al.* Crystal structure of a light-driven sodium pump. *Nat. Struct. Mol. Biol.***22**, 390–396 (2015).

19. Yutin, N. & Koonin, E. Vl (Ecoles Universitaires de Recherche) CBH-EUR-GS (ANR-17-EURE-0003). The reported study (particularly, spectroscopy of the protein crystals) was funded by RFBR and CNRS according to the research project № 19-52-15017. FR-V thanks the grant 'VIREVO' CGL2016-76273-P [AEI/FEDER, EU], (co-funded with FEDER funds).Measurements of electrogenic properties were supported by RFBR grant 18-04-00503a (to SS). Bioinformatics search of new heliorhodopsins (including viral proteins) was supported by RSF project 19-44-06302.

Author contributions: DV made cloning, expression, purification and functional characterization of the protein and cloning, expression and flash-photolysis investigation of the 48C12 and E230Q and E149Q mutants; IC helped with spectroscopy data analysis; RA performed crystallization; AA made bioinformatics analysis; KK did spectroscopic studies of the crystals; KK and RA collected the diffraction data with the help of GB; KK solved the structures; IG helped with structure solving, refinement and analysis; AA performed sequence alignment analysis; SS and MM performed the electrometric time-resolved measurements of the membrane potential, SS analyzed the data; JMH-M performed genome analysis of Ca. Actinomarinales; GB, AP, AR, VB, EB, SS and FR-V contributed to data analysis and editing the manuscript; VG designed and supervised the project; KK and VG analyzed the results and prepared the manuscript with input from all the o. Proteorhodopsin genes in giant viruses. *Biol. Direct* (2012). doi:10.1186/1745-6150-7-34

20. Bratanov, D. *et al.* Unique structure and function of viral rhodopsins. *Nat. Commun.***10**, 4939 (2019).

21. Needham, D. M. *et al.* A distinct lineage of giant viruses brings a rhodopsin photosystem to unicellular marine predators. *Proc. Natl. Acad. Sci.* (2019). doi:10.1073/pnas.1907517116

22. Béja, O., Spudich, E. N., Spudich, J. L., Leclerc, M. & DeLong, E. F. Proteorhodopsin phototrophy in the ocean. *Nature* (2001). doi:10.1038/35081051

23. Inoue, K. *et al.* A natural light-driven inward proton pump. *Nat. Commun.* (2016). doi:10.1038/ncomms13415

24. Shevchenko, V. *et al.* Inward H+ pump xenorhodopsin: Mechanism and alternative optogenetic approach. *Sci. Adv.* (2017). doi:10.1126/sciadv.1603187

25. Pushkarev, A. *et al.* A distinct abundant group of microbial rhodopsins discovered. *Nature* (2018). doi:10.1038/s41586-018-0225-9

26. Singh, M., Inoue, K., Pushkarev, A., Béjà, O. & Kandori, H. Mutation Study of Heliorhodopsin 48C12. *Biochemistry* (2018). doi:10.1021/acs.biochem.8b00637

27. Flores-Uribe, J. *et al.* Heliorhodopsins are absent in diderm (Gram-negative) bacteria: Some thoughts and possible implications for activity. *Environmental Microbiology Reports* (2019). doi:10.1111/1758-2229.12730

28. Shihoya, W. *et al.* Crystal structure of heliorhodopsin. *Nature* (2019). doi:10.1038/s41586-019-1604-6

29. Volkov, O. *et al.* Structural insights into ion conduction by channelrhodopsin 2. *Science (80-.).***358**, (2017).

30. von HEIJNE, G. & GAVEL, Y. Topogenic signals in integral membrane proteins. *Eur.*

J. Biochem. (1988). doi:10.1111/j.1432-1033.1988.tb14150.x

31. Ho, B. K. & Gruswitz, F. HOLLOW: Generating accurate representations of channel and interior surfaces in molecular structures. *BMC Struct. Biol.***8**, (2008).

32. Gerwert, K., Freier, E. & Wolf, S. The role of protein-bound water molecules in microbial rhodopsins. *Biochimica et Biophysica Acta - Bioenergetics* (2014). doi:10.1016/j.bbabio.2013.09.006

33. Drachev, L. A. *et al.* Direct measurement of electric current generation by cytochrome oxidase, H+-ATPase and bacteriorhodopsin. *Nature* (1974). doi:10.1038/249321a0

34. DRACHEV, L. A., KAULEN, A. D., KHITRINA, L. V. & SKULACHEV, V. P. Fast Stages of Photoelectric Processes in Biological Membranes: I. Bacteriorhodopsin. *Eur. J. Biochem.* (1981). doi:10.1111/j.1432-1033.1981.tb06361.x

35. Siletsky, S. A. *et al.* Electrogenic steps of light-driven proton transport in ESR, a retinal protein from Exiguobacterium sibiricum. *Biochim. Biophys. Acta - Bioenerg.* (2016). doi:10.1016/j.bbabio.2016.08.004

36. Kovalev, K. *et al.* Structure and mechanisms of sodium-pumping KR2 rhodopsin. *Sci. Adv.***5**, eaav2671 (2019).

37. Der, A. *et al.* Alternative translocation of protons and halide ions by bacteriorhodopsin. *Proc. Natl. Acad. Sci.* (2006). doi:10.1073/pnas.88.11.4751

38. Harris, A. *et al.* A new group of eubacterial light-driven retinal-binding proton pumps with an unusual cytoplasmic proton donor. *Biochim. Biophys. Acta - Bioenerg.* (2015). doi:10.1016/j.bbabio.2015.08.003

39. Okumura, H., Murakami, M. & Kouyama, T. Crystal structures of acid blue and alkaline purple forms of bacteriorhodopsin. *J. Mol. Biol.* (2005). doi:10.1016/j.jmb.2005.06.026

40. Singh, M., Katayama, K., Béjà, O. & Kandori, H. Anion binding to mutants of the Schiff base counterion in heliorhodopsin 48C12. *Phys. Chem. Chem. Phys.* (2019). doi:10.1039/C9CP04102H

41. Moukhametzianov, R. *et al.* Development of the signal in sensory rhodopsin and its transfer to the cognate transducer. *Nature***440**, 115–119 (2006).

42. Mitchell, A. L. *et al.* InterPro in 2019: improving coverage, classification and access to protein sequence annotations. *Nucleic Acids Res.* (2019). doi:10.1093/nar/gky1100

43. Zhou, J. *et al.* Microbial mediation of carbon-cycle feedbacks to climate warming. *Nat. Clim. Chang.* (2012). doi:10.1038/nclimate1331

44. Gordeliy, V. I. *et al.* Molecular basis of transmembrane signalling by sensory rhodopsin II-transducer complex. *Nature***419**, 484–487 (2002).

45. Seidel, R. *et al.* The primary structure of sensory rhodopsin II: a member of an additional retinal protein subgroup is coexpressed with its transducer, the halobacterial transducer of rhodopsin II. *Proc. Natl. Acad. Sci.* (1995). doi:10.1073/pnas.92.7.3036

46. Jung, K. H., Trivedi, V. D. & Spudich, J. L. Demonstration of a sensory rhodopsin in eubacteria. *Mol. Microbiol.* (2003). doi:10.1046/j.1365-2958.2003.03395.x

47. Sutcliffe, I. C. New insights into the distribution of WXG100 protein secretion systems. *Antonie van Leeuwenhoek, Int. J. Gen. Mol. Microbiol.* (2011). doi:10.1007/s10482-010-9507-4

48. Studier, F. W. Protein production by auto-induction in high-density shaking cultures. *Protein Expr. Purif.* (2005). doi:10.1016/j.pep.2005.01.016

49. Chizhov, I. & Engelhard, M. Temperature and halide dependence of the photocycle of halorhodopsin from Natronobacterium pharaonis. *Biophys. J.***81**, 1600–1612 (2001).

50. Chizhov, I. *et al.* The photophobic receptor from Natronobacterium pharaonis: Temperature and pH dependencies of the photocycle of sensory rhodopsin II. *Biophys. J.***75**, 999–1009 (1998).

51. Chizhov, I. *et al.* Spectrally silent transitions in the bacteriorhodopsin photocycle. *Biophys. J.***71**, 2329–2345 (1996).

52. Gordeliy, V. I. *et al.* Crystallization in Lipidic Cubic Phases: A Case Study with Bacteriorhodopsin. in *Membrane Protein Protocols* (2003). doi:10.1385/1-59259-400-x:305

53. Von Stetten, D. *et al.*In crystallo optical spectroscopy (icOS) as a complementary tool on the macromolecular crystallography beamlines of the ESRF. *Acta Crystallogr. Sect. D Biol. Crystallogr.* (2015). doi:10.1107/S139900471401517X

54. Kabsch, W. XDS. *Acta Crystallogr D Biol Crystallogr* (2010). doi:10.1107/S0907444909047337

55. Winn, M. D. *et al.*Overview of the *CCP* 4 suite and current developments. *Acta Crystallogr. Sect. D Biol. Crystallogr.* (2011). doi:10.1107/S0907444910045749

56. Källberg, M. *et al.* Template-based protein structure modeling using the RaptorX web server. *Nat. Protoc.* (2012). doi:10.1038/nprot.2012.085

57. Terwilliger, T. C. *et al.* Phenix.mr-rosetta: Molecular replacement and model rebuilding with Phenix and Rosetta. *J. Struct. Funct. Genomics* (2012). doi:10.1007/s10969-012-9129-3

58. Adams, P. D. *et al.* PHENIX: A comprehensive Python-based system for macromolecular structure solution. *Acta Crystallogr. Sect. D Biol. Crystallogr.* (2010). doi:10.1107/S0907444909052925

59. Murshudov, G. N. *et al.* REFMAC5 for the refinement of macromolecular crystal structures. *Acta Crystallogr. D. Biol. Crystallogr.***67**, 355–367 (2011).

60. Emsley, P. & Cowtan, K. Coot: model-building tools for molecular graphics. *Acta Crystallogr. Sect. D Biol. Crystallogr.***60**, 2126–2132 (2004).

61. Lomize, M. A., Pogozheva, I. D., Joo, H., Mosberg, H. I. & Lomize, A. L. OPM database and PPM web server: Resources for positioning of proteins in membranes. *Nucleic Acids Res.***40**, (2012).

62. Chojnacki, S., Cowley, A., Lee, J., Foix, A. & Lopez, R. Programmatic access to bioinformatics tools from EMBL-EBI update: 2017. *Nucleic Acids Res.* (2017). doi:10.1093/nar/gkx273

63. Ciccarelli, F. D. *et al.* Toward automatic reconstruction of a highly resolved tree of life. *Science (80-.).* (2006). doi:10.1126/science.1123061

64. Huang, Y., Niu, B., Gao, Y., Fu, L. & Li, W. CD-HIT Suite: A web server for clustering and comparing biological sequences. *Bioinformatics* (2010). doi:10.1093/bioinformatics/btq003

65. Hyatt, D. *et al.* Prodigal: prokaryotic gene recognition and translation initiation site identification. *BMC Bioinformatics* (2010). doi:10.1186/1471-2105-11-119

66. Lowe, T. M. & Eddy, S. R. TRNAscan-SE: A program for improved detection of transfer RNA genes in genomic sequence. *Nucleic Acids Res.* (1996). doi:10.1093/nar/25.5.0955

67. Nawrocki, E. P. Structural RNA Homology Search and Alignment using Covariance Models. *Ph.D. thesis* (2009).

68. Huang, Y., Gilna, P. & Li, W. Identification of ribosomal RNA genes in metagenomic fragments. *Bioinformatics* (2009). doi:10.1093/bioinformatics/btp161

69. Buchfink, B., Xie, C. & Huson, D. H. Fast and sensitive protein alignment using DIAMOND. *Nature Methods* (2014). doi:10.1038/nmeth.3176

70. Tatusov, R. L. *et al.* The COG database: new developments in phylogenetic classification of proteins from complete genomes. *Nucleic Acids Res.* (2001).

71. Haft, D. H. *et al.* TIGRFAMs: a protein family resource for the functional identification of proteins. *Nucleic Acids Res.* (2001).

72. Eddy, S. R. Accelerated profile HMM searches. *PLoS Comput. Biol.* (2011). doi:10.1371/journal.pcbi.1002195

Acknowledgments

General: We thank O. Volkovand A.Yuzhakova for technical assistance. We acknowledge the Structural Biology Groups of the Swiss Light Source (SLS, Villigen, Switzerland), SOLEIL (Saint-Aubin, France) and PETRAIII (Hamburg, Germany) for granting access to the synchrotron beamlines. We are grateful to A. Royant (ID29S Cryobench laboratory, ESRF) for help with collection of the 48C12 crystals optical absorption spectra.

Funding: This work was supported by the common program of Agence Nationale de la Recherche (ANR), France and Deutsche Forschungsgemeinschaft, Germany (ANR-15-CE11-0029-02/FA 301/11-1 and MA 7525/1-1) and by funding from Frankfurt: Cluster of Excellence Frankfurt Macromolecular Complexes by the Max Planck Society (to EB) and by the Commissariat à l'EnergieAtomique et aux Energies Alternatives (Institut de Biologie Structurale) – Helmholtz-Gemeinschaft Deutscher Forschungszentren (Forschungszentrum Jülich) Special Terms and Conditions 5.1 specific agreement. This work used the platforms of the Grenoble Instruct-ERIC center (ISBG; UMS 3518 CNRS-CEA-UJF-EMBL) within the Grenoble Partnership for Structural Biology (PSB). Platform access was supported by FRISBI (ANR-10-INBS-05-02) and GRAL, a project of the University Grenoble Alpes graduate school (Ecoles Universitaires de Recherche) CBH-EUR-GS (ANR-17-EURE-0003). The reported study (particularly, spectroscopy of the protein crystals) was funded by RFBR and CNRS according to the research project № 19-52-15017. FR-V thanks the grant 'VIREVO' CGL2016-76273-P [AEI/FEDER, EU], (co-funded with FEDER funds).Measurements of electrogenic properties were supported by RFBR grant 18-04-00503a (to SS). Bioinformatics search of new heliorhodopsins (including viral proteins) was supported by RSF project 19-44-06302.

Author contributions: DV made cloning, expression, purification and functional characterization of the protein and cloning, expression and flash-photolysis investigation of the 48C12 and E230Q and E149Q mutants; IC helped with spectroscopy data analysis; RA performed crystallization; AA made bioinformatics analysis; KK did spectroscopic studies of the crystals; KK and RA collected the diffraction data with the help of GB; KK solved the structures; IG helped with structure solving, refinement and analysis; AA performed sequence alignment analysis; SS and MM performed the electrometric time-resolved measurements of the membrane potential, SS analyzed the data; JMH-M performed genome analysis of Ca. Actinomarinales; GB, AP, AR, VB, EB, SS and FR-V contributed to data analysis and editing the manuscript; VG designed and supervised the project; KK and VG analyzed the results and prepared the manuscript with input from all the other authors.

Competing interests: Authors declare no competing interests

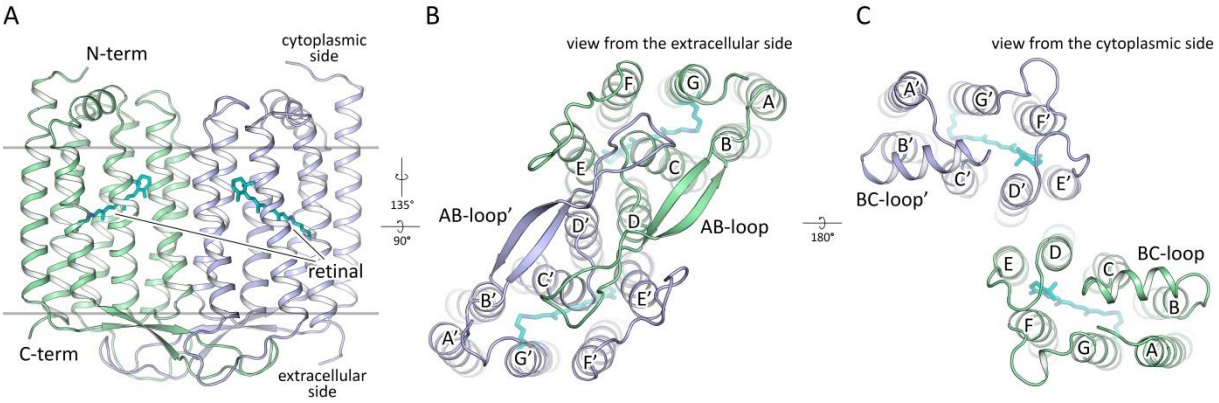

Fig. 1.Overall architecture of the heliorhodopsin48C12 dimer.A. Side view of the dimer. Hydrophobic/hydrophilic membrane boundaries are shown with gray lines. **B.** View from the extracellular side. **C.** View from the cytoplasmic side. Cofactor retinal is colored teal.

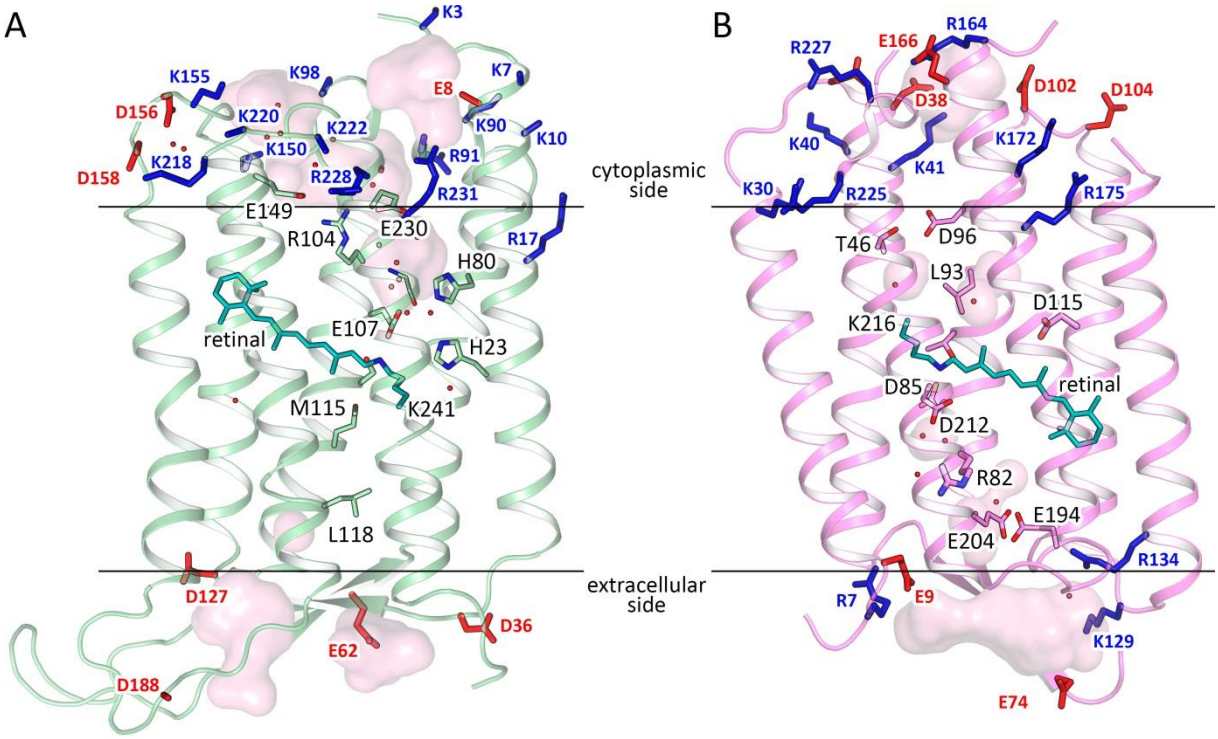

Fig. 2.Comparison of 48C12 (green) and bR (purple, PDB ID 1C3W). A. Side view of the heliorhodopsin 48C12. N-terminus is at the cytoplasmic side of the membrane. **B.** Side view of the bR. N-terminus is at the extracellular side of the membrane. Hydrophobic/hydrophilic membrane boundaries are shown with black lines. Positively and negatively charged residues on the protein cytoplasmic and extracellular surfaces are shown in blue and red, respectively.

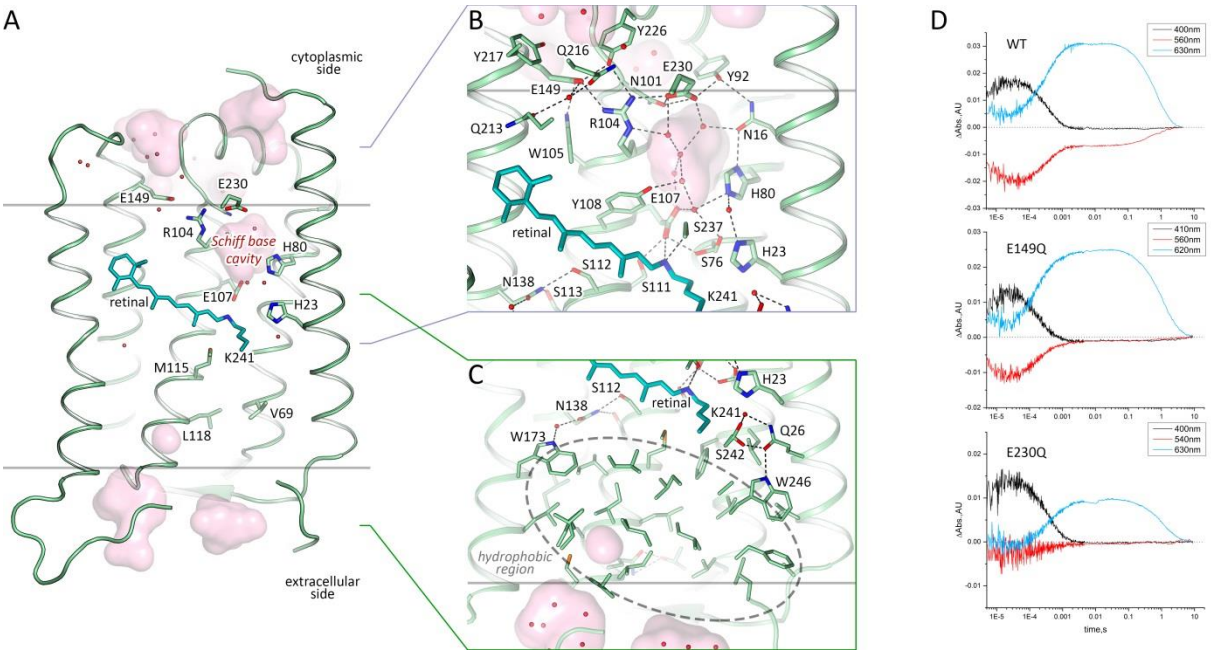

Fig. 3.Structure of the 48C12 protomer. A. Side view of the protomer in the membrane. **B.** Detailed view of the cytoplasmic part. **C.** Detailed view of the extracellular sideand the hydrophobic region. Cofactor retinal is colored teal. Hydrophobic/hydrophilic membrane boundaries are shown with gray lines. Cavities are calculated with HOLLOW[31]and shown in pink. Charged residues in 48C12 are shown with thicker sticks. Helices F and G are not shown. **D.** Time evolution of the transient absorption changes of photo-excited 48C12, wild type (WT), E230Q and E149Q mutant forms. The characteristic wavelengths of intermediate states are slightly shifted in the mutants. The O_2-state decay is almost two times longer in both48C12 variants.

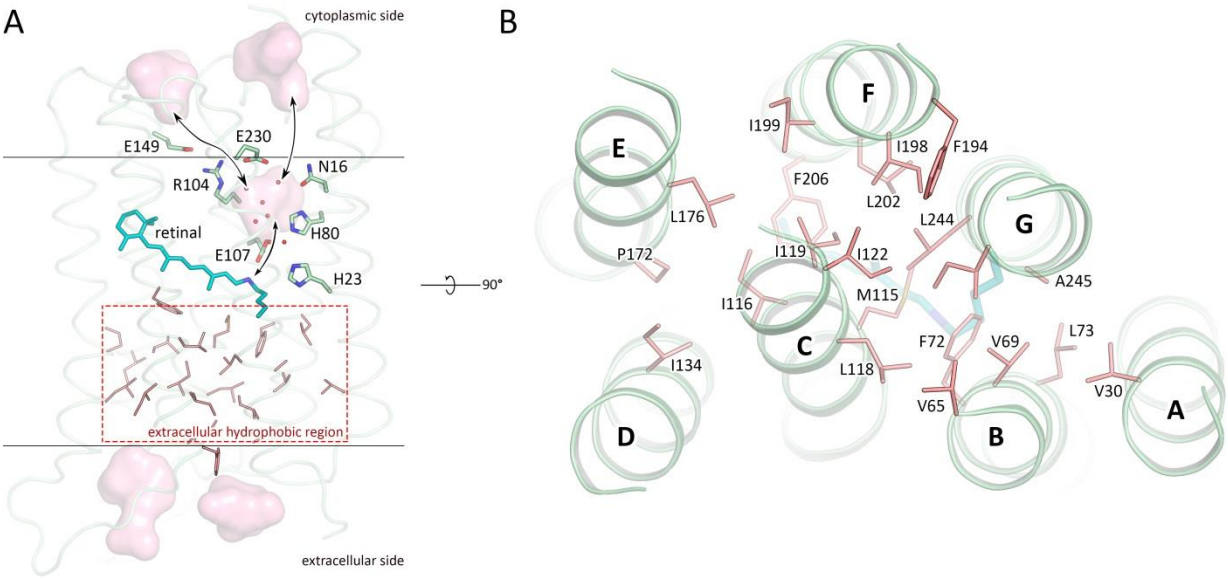

Fig. 4.Hydrophobic residues in the extracellular part of 48C12. A. Side view of the 48C12 protomer. The residues comprising the extracellular hydrophobic region are colored red. The region is embedded in the extracellular half of the lipid bilayer and is contoured with dashed red rectangle. Membrane core boundaries are shown with black lines. Black arrows indicate putative pathways connecting the inner cavity (SBC), cytoplasmic side of the protein and RSB. Cavities are colored pink. Water molecules in the inner cavity are shown with red spheres. **B.** View on the hydrophobic region from the extracellular surface of the protein. Loops are hidden for clarity. Hydrophobic residues in the extracellular internal part of the 48C12 protomer are colored red. Cofactor retinal is colored teal.

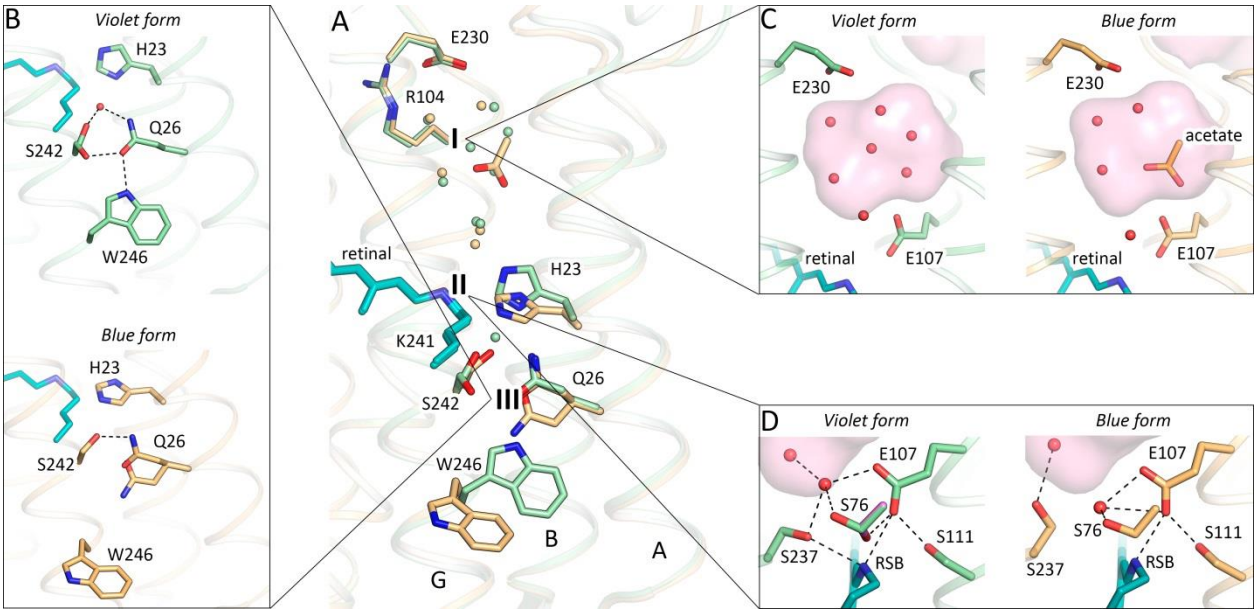

Fig. 5.Comparison of the violet (shown in green) and blue (shown in orange) forms of 48C12. A. Alignment of the two models. Three most notable differences between two structures are: I –the cavity at the cytoplasmic side; II – rearrangements of the residues near the RSB; III – loss of the water molecule between His23 and Ser242 in the blue form and rearrangements of the Gln26 and Trp246 side chains. Water molecules are shown with the spheres and colored green and orange, corresponding to the violet and blue forms of 48C12, respectively. **B.** Detailed view of the Ser242-Gln26-Trp246 cluster and His23 in the violet and blue forms. **C.** Detailed view of the cavity (active site) at the cytoplasmic side in the violet and blue forms. **D.** Detailed view of the RSB and surrounding residues in the violet and blue forms. In violet form, Ser76 assumestwo alternative conformations (second is colored magenta for clarity). Cavities are colored pink.

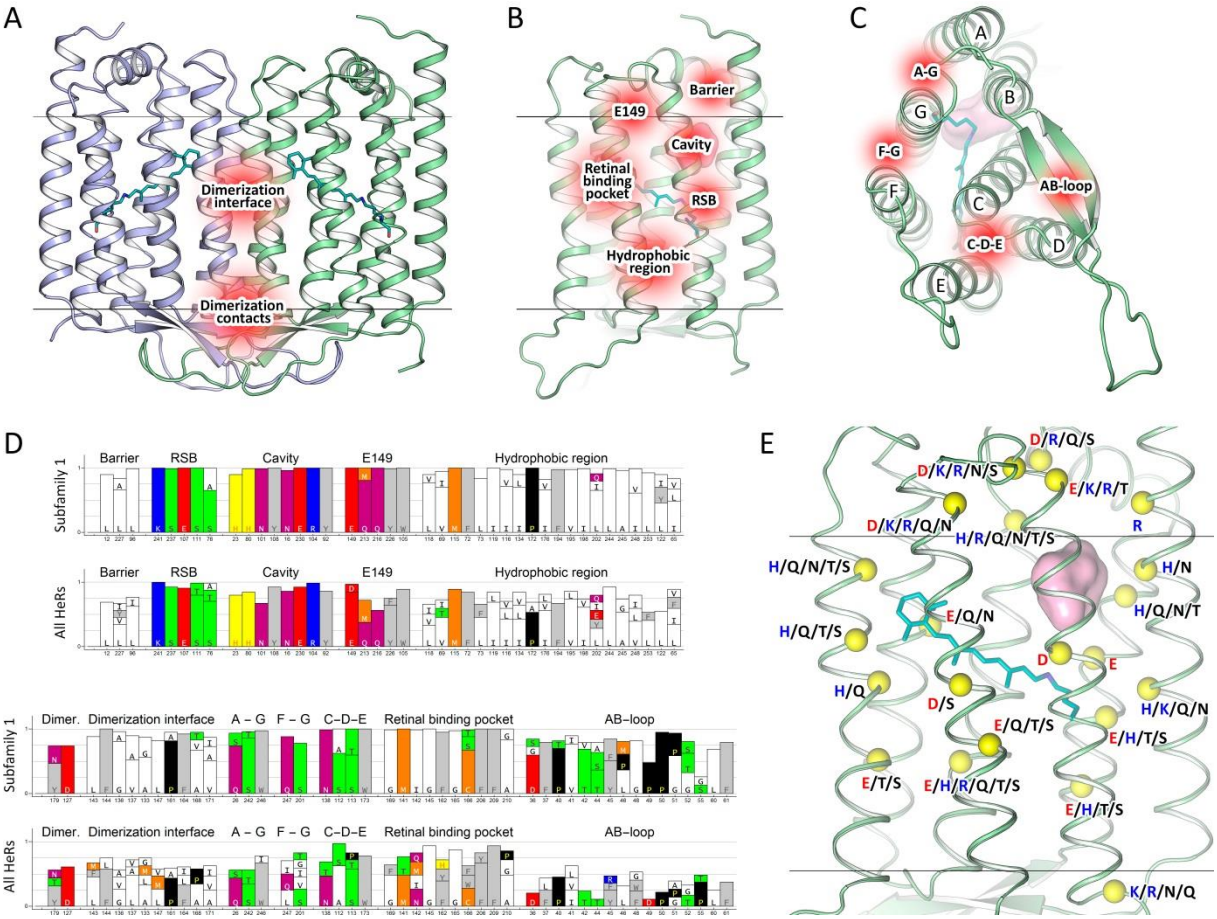

Fig. 6. Key regions of 48C12 and heliorhodopsins family identified by structure-based bioinformatical analysis. A. View of the 48C12 dimer with identified regions (shown in red) comprised of conservative residues of the dimerization interface (polar, responsible for contacts between protomers and hydrophobic, responsible for hydrophobic interaction inside the membrane).**B.** View of the 48C12 protomer with the key regions (shown in red), comprised of conservative residues. **C.** View of the 48C12 protomer with the polar clusters (shown in red), shown to be conservative among subfamily 1 and most of other subfamilies. **D.** Most conservative residues among subfamily 1 and all HeRs, comprising the key regions of 48C12. **E.** The location of the residues in 48C12, which are probable analogues of charged or polar residues in other subfamilies of HeRs (selected using a sequence alignment, See SI Appendix, fig. S16, S17). The backbone carbon atoms of these residues are shown with yellow spheres. The polar cavity in the cytoplasmic part is shown with a pink surface. Cofactor retinal is colored teal.